

A strong optical flare before the rising afterglow of GRB 080129

J. Greiner¹, T. Krühler¹, S. McBreen¹, M. Ajello^{1,2}, D. Giannios³, R. Schwarz⁴, S. Savaglio¹, A. Küpcü Yoldaş⁵, C. Clemens¹, A. Stefanescu¹, G. Sala^{1,6}, F. Bertoldi⁷, G. Szokoly⁸, S. Klose⁹

ABSTRACT

We report on GROND observations of a 40 sec duration (rest-frame) optical flare from GRB 080129 at redshift 4.349. The rise- and decay time follow a power law with indices +12 and -8, respectively, inconsistent with a reverse shock and a factor 10^5 faster than variability caused by ISM interaction. While optical flares have been seen in the past (e.g. GRB 990123, 041219B, 060111B and 080319B), for the first time, our observations not only resolve the optical flare into sub-components, but also provide a spectral energy distribution from the optical to the near-infrared once every minute. The delay of the flare relative to the GRB, its spectral energy distribution as well as the ratio of pulse widths suggest it to arise from residual collisions in GRB outflows (Li & Waxman 2008). If this interpretation is correct and can be supported by more detailed modelling or observation in further GRBs, the delay measurement provides an independent, determination of the Lorentz factor Γ of the outflow.

Subject headings: gamma-rays: bursts – radiation mechanisms: non-thermal

¹Max-Planck-Institut für Extraterrestrische Physik, Giessenbachstraße 1, 85740 Garching, Germany; jcg, kruehler, smcbreen, savaglio, cclemens, astefan@mpe.mpg.de

²Present address: Stanford Univ., Stanford, CA 94305, U.S.A.; majello@slac.stanford.edu

³Max-Planck-Institut für Astropysik, 85740 Garching, Germany; giannios@mpa-garching.mpg.de

⁴Astrophysical Institute Potsdam, 14482 Potsdam, An der Sternwarte 16, Germany; schwarz@aip.de

⁵Present address: ESO, 85740 Garching, Schwarzschild-Str. 2, Germany; ayoldas@eso.org

⁶Present address: Dept. de Física i Enginyeria Nuclear, EUETIB, Univ. Politècnica de Catalunya, c/ Compte d'Urgell 187, 08036 Barcelona, Spain; gloria.sala@upc.edu

⁷Astron. Inst. Univ. Bonn, Auf dem Hügel 71, 53121 Bonn, Germany; bertoldi@astro.uni-bonn.de

⁸Eötvös Univ., 1117 Budapest, Pazmany P. stny. 1/A, Hungary; szgyula@elte.hu

⁹Thüringer Landessternwarte, Sternwarte 5, 07778 Tautenburg, Germany; klose@tls-tautenburg.de

1. Introduction

Long-duration gamma-ray bursts (GRBs) emit their bulk luminosity over a time period of 2-50 sec in the 100-1000 keV range (e.g. (Kaneko et al. 2006)). Their afterglows are generally assumed to arise from the interaction of the blast wave with the surrounding interstellar material (ISM), where a strong relativistic shock is driven (so-called external shock). This happens about 10^2 - 10^4 sec after the burst, at distances of the order of 3×10^{16} cm (Meszaros & Rees 1997). The shocked gas is the source of a long-lived, slowly decaying afterglow emission.

Some afterglows have shown substantial optical variability, both at early times as well as at late times. The early ones can be distinguished into a component which tracks the prompt gamma-rays (GRB 041219A (Vestrand et al. 2005; Blake et al. 2005), GRB 050820A (Vestrand et al. 2006), GRB 080319B (Racusin et al. 2008)) and an afterglow component which starts during or shortly after the prompt phase (GRB 990123 (Akerlof et al. 1999), GRB 030418 (Rykoff et al. 2004), GRB 060111B (Klotz et al. 2006)). The former component has been attributed to internal shocks, while the latter component was interpreted as reverse shock emission, e.g. (Sari & Piran 1999a; Meszaros & Rees 1999). At late times, some GRB afterglows (021004, 030329) showed bumps on top of the canonical fading, with timescales of 10^4 - 10^5 sec. Originally, these bumps have been interpreted as the interaction of the fireball with moderate density enhancements in the ambient medium, with a density contrast of order 10 (Lazzati et al. 2002), and later by additional energy injection episodes (Björnsson et al. 2004).

The optical variability due to the interaction with the ISM is expected to be not faster than 10^6 sec, because the blast wave, once it has swept up enough interstellar material to produce the canonical afterglow emission, is thought to be only mildly relativistic. This is different with optical emission possibly related to the forward or reverse shock: here the emission is relativistic, and the timescales in the observer frame are shortened by Γ^{-2} , with Γ being the bulk Lorentz factor which typically is assumed to be 300–500. The reverse shock is predicted to happen with little delay with respect to the gamma-ray emission unless the Lorentz factor is very small, and the corresponding optical emission has a decay-time power law index of -2 for a constant density environment, or up to -2.8 for a wind density profile (Kobayashi 2000).

Swift/BAT triggered on GRB 080129 (trigger 301981) at 06:06:46 UT (Immler et al. 2008) which had an observed duration $T_{90}=48$ sec. BAT measured a fluence (over T_{90} , the time

during which 90% of the fluence is emitted) of 8.9×10^{-7} erg/cm² in the 15-150 keV band¹. The spectral slope is 1.3 with no spectral turn-over up to 150 keV. If we assume the expected spectral turn-over according to a canonical GRB spectrum to be at $E_{peak} = 300$ (500) keV, the total isotropic gamma-ray energy equivalent is $E_{\gamma(iso)} = 6.5(7.7) \times 10^{52}$ erg (15–1000 keV). At 320 sec after the trigger, Swift slewed to a different location on the sky, placing the line-of-sight towards the GRB nearly in the BAT detector plane, therefore being blind to any late emission. Pointed observations of the GRB with the X-ray telescope (XRT) and the UV-optical telescope (UVOT) started only at 07:00:08 UT, 3.2 ksec after the GRB trigger. A clearly fading X-ray source was discovered, but no emission seen with UVOT (Holland 2008).

We started optical/near-infrared (NIR) imaging with GROND immediately after the trigger, and had independently identified the optical/NIR afterglow (Krühler et al. 2008) though we reported it after Bloom (2008). Here we report the full results.

2. Observations and Results

2.1. Optical/NIR photometry

GROND, a simultaneous 7-channel imager (Greiner et al. 2008) mounted at the 2.2 m MPI/ESO telescope at La Silla (Chile), started observing the field at 06:10:18 UT, about 4 min after the GRB. Our imaging sequence began with 46 sec integrations in the $g'r'i'z'$ channels, spaced at about 50 sec due to detector read-out and preset to a new telescope dither position. After about 10 min, the exposure time was increased to 137 sec, and after another 28 min to 408 sec. Since the afterglow brightness was rising, the exposure time was reduced back to 137 sec at 07:21 for the rest of the night. In parallel, the three near-infrared channels JHK were operated with 10 sec integrations, separated by 5 sec due to read-out, data-transfer and K -band mirror movement.

The first images immediately revealed a strongly flaring source. The light curve of the afterglow (Fig. 1) shows this unique pattern in more detail: there is a ≈ 3 mag amplitude flare of 80 sec (full-width at half maximum; FWHM) duration, peaking at ≈ 540 sec post-burst.

Thereafter, the afterglow brightness is continuously rising until 6000 sec after the GRB. At the beginning of the next night, at 65 ksec after the GRB, the afterglow intensity is still at the same level, despite declining by a factor of 25 at X-rays. In contrast, in the 65 - 500

¹<http://gcn.gsfc.nasa.gov/gcn/notices.s/301981>

ksec interval the emission in the optical/NIR and X-rays is correlated, with a slow rise ($t^{0.15}$) over another day, and a subsequent rapid decay ($t^{-2.0}$).

2.2. Optical spectroscopy

We obtained an optical spectrum of the afterglow of GRB 080129 in the 500-800 nm region with FORS1/VLT (Fig. 3) on Jan 30, 2008, 06:16 (mid-time) consisting of 4 exposures of 1800 sec each. The strong fringing of the blue-sensitive detector long-wards of 7500 Å and the strong foreground extinction of $A_V=3.4$ mag result in a limited range of the spectrum being useful for analysis; but luckily Ly α and some metal absorption lines like SiII (1260 Å) and SiIV (1402 Å) happen to fall in this usable range, so that a redshift of $z=4.349\pm 0.002$ (luminosity distance of 40 Gpc in concordance cosmology) could be derived.

2.3. NIR high time-resolution photometry

Observations with VLT/ISAAC (ESO Paranal, Chile) and NTT/SOFI (ESO La Silla, Chile) were triggered to monitor GRB 080129 in the NIR with high-time resolution photometry. ISAAC was used in FastPhot mode in J band on 2008 Jan 30, between UT 00:34 and 02:35, with 14.3 ms exposures, while SOFI was used thereafter from UT 03:30 to 05:04 with 40.1 ms exposures (also FastPhotJitt mode in J band). After bias and flatfield correction and background subtraction the frames were stacked to achieve longer total integration times (4000 frames combined give 57.2 s integration time in ISAAC, 1000 frames combined give 40 s integration time in SOFI). The light curves do not show any flaring activity above 0.3 mag amplitude.

2.4. Sub-millimeter observations

For the photometric observations at 1.2 mm (250 GHz) we used the 117 channel Max-Planck Bolometer array MAMBO-2 (Kreysa et al. 1998) at the IRAM 30 m telescope on Pico Veleta, Spain. MAMBO-2 has a half-power spectral bandwidth from 210 to 290 GHz, with an effective bandwidth center for flat spectra of 249 ± 1 GHz (1.20 mm, 2 ± 2 mm precipitable water vapor). The effective beam FWHM is 10.7 arcsec, and the undersampled field of view is 4 arcmin. Atmospheric conditions were generally good during the observations, with typical line of sight opacities between 0.2 and 0.3 and low sky noise. The on sky integration times varied between 1200 and 5000 sec on the five epochs. Observations were performed using

the standard on-off technique, with the sub-reflector switching every 0.25 seconds between two sky positions (on and off source) separated by 32 arcsec. The telescope pointing was frequently checked on a nearby quasar and was found to be stable within 2 arcsec. The data were analyzed using the MOPSIC software package. Correlated noise was subtracted from each channel using the weighted average signals from the surrounding channels. Absolute flux calibration was done through observations of planets, resulting in a flux calibration uncertainty of about 20%. The third–fifth epochs on Feb 3, 6 and 10 yielded only upper limits of <0.5 mJy (3σ) (see Tab. 1).

3. Discussion

3.1. The rising afterglow

The rising light curve between 1000-6000 sec after the GRB is likely the emerging afterglow. The rather steep power law photon index of $\alpha = -1.35 \pm 0.15$ and the flux rise ($F \sim t^\beta$) with $\beta \sim 1$ indicate that the characteristic synchrotron frequency has already crossed the optical band at $t=1000$ sec. Our interpretation for the rising part is that the ejecta have not entered the deceleration phase at $t=6000$ sec. In this case one can use the peak time of the light curve at $t \gtrsim 6000$ sec, to estimate the fireball Lorentz factor at the time of the deceleration which is expected to be half of the initial Lorentz factor Γ_0 (Sari & Piran 1999b; Panaitescu & Kumar 2000; Molinari et al. 2007). Using the formulation of (Molinari et al. 2007), we obtain for the ISM case $\Gamma_0 \approx 130 \left(\frac{E_{53}}{\eta_{0.2} n} \right)^{1/8}$, where $\eta = 0.2\eta_{0.2}$ is the radiative efficiency (Bloom et al. 2003). Ignoring the weak dependence on η and the external density n , and using our above derived $E_{53}=0.7$, we get $\Gamma_0 \approx 120$ (with allowed values down to 85 if the peak emission was at 15.000 sec instead of 6.000 sec).

3.2. The late decay light curve

At very late times, starting at 180 ksec after the GRB, the X-ray and optical/NIR emission vary achromatically. Again, this is in contrast to the behaviour in most Swift GRBs (Panaitescu 2007), but the steepening of the decay to $\alpha \sim -2$ and the spectrum by $\delta\alpha \sim 0.5$ (Tab. 2) is consistent with a jet break. The jet angle Θ was calculated following Sari et al. (1999) for the ISM model and Bloom et al. (2003) for the wind model, where in the former case the redshift factor was added:

$$\Theta_{\text{ISM}} = \frac{1}{6} \left(\frac{t_b}{1+z} \right)^{3/8} \left(\frac{n \eta_{0.2}}{E_{52}} \right)^{1/8} \quad (1)$$

$$\Theta_{\text{wind}} = 0.169 \left(2 \frac{t_b}{1+z} \right)^{1/4} \left(\frac{\eta_{0.2} A_\star}{E_{52}} \right)^{1/4}, \quad (2)$$

Using $E_{\text{iso}} = 6.5(7.7) \times 10^{52}$ erg/s (see introduction), our derived redshift, a circumburst density $n = 1 \text{ cm}^{-3}$, and a break time of $t_b = 180000 \text{ sec} = 2.08 \text{ days}$, as well as the canonical values $A_\star = 1$ and $\eta_{0.2} = 1$, we derive a jet opening angle of $4^\circ.35(4^\circ.26)$ for ISM and $3^\circ.82(3^\circ.66)$ for a wind medium (where the density follows Ar^{-2} , with $A = \dot{M}/4\pi v = 5 \times 10^{11} A_\star \text{ g cm}^{-1}$ derived for the reference values $\dot{M} = 1 \times 10^{-5} M_\odot \text{ yr}^{-1}$ and $v = 1000 \text{ km s}^{-1}$). The beaming factor is $b \approx \Theta^2/2$. The corresponding jet angle-corrected energy is $1.88(2.13) \times 10^{50}$ erg/s for ISM, and $1.44(1.57) \times 10^{50}$ erg/s for wind medium.

3.3. The plateau

This GRB is remarkable for a second reason: it showed a prolonged plateau phase in its afterglow emission, most pronounced in the X-ray band. Flat, or shallow-decay parts of the light curve are now commonly detected in the Swift era (Liang et al. 2007), and occur between 100 sec until 10^3 - 10^5 sec after the burst. In GRB 080129, we observe the plateau to last from 9000 - 56000 sec in the rest frame (50000 - 300.000 sec observers frame), so starting substantially later, but with a duration (in the rest frame) which is not extraordinary. However, the stunning fact is that this same plateau is also seen in the optical/NIR data of GROND. Using also the MAMBO detection at 1.2 mm, the overall spectrum during the plateau cannot be fit by a single power law, but requires a second component. Adopting a broken power law, at least one break is required, with the break energy between the optical (400 nm) and X-rays (0.5 keV). The best-fit power law indices are 1.57 ± 0.06 for the MAMBO-GROND spectrum, and $2.36_{-0.58}^{+1.01}$ for the high-frequency part of the spectrum. Integrating this spectrum over the duration of the plateau phase (69 hrs) results in a total emitted energy, of 3.4×10^{52} erg, about 50% of the total energy emitted during T_{90} in the 15–150 keV band.

3.4. The flare

3.4.1. Non-favored explanations

The optical flare is more difficult to explain due to primarily two facts: it is not correlated to the gamma-ray emission, but delayed by $12 \times T_{90}$, and it occurs well before the peak of the optical afterglow. One possibility is to assume that it is the prompt emission of the GRB while BAT triggered on the precursor. The typical ratio of at least 30 for the gamma-ray

fluence of proper burst to precursor (Lazzati 2005) implies $E_{\gamma(iso)} = 2.0(2.3) \times 10^{54}$ erg, similar to the brightest previously known burst GRB 990123 (Akerlof et al. 1999), therefore making the precursor hypothesis unlikely.

Another possibility to explain the optical flare is as the reverse shock emission. In a constant density environment, a reverse shock (Kobayashi 2000) is expected to rise rapidly ($\beta_{rise} = 3p - 3/2$, where p is the powerlaw index of the electron distribution), and decline, in the thin shell case, with $\beta_{decline} = -(27p + 7)/35$. With the canonical range of $p = 2.2 - 2.5$, this implies $\beta_{rise} = 5.1 - 6.0$, and $\beta_{decline} = -1.9 - -2.1$, in contrast to our observed values of $\beta_{rise} = 12.1 \pm 1.5$ and $\beta_{decline} = 8.3 \pm 1.8$. While this is true only for the simplest model, and the actual rise and decline values depend on the density profile and the p values of the electron distribution, we are not aware of any reverse shock model that gives so steep flux density variations. Note also that a wind profile, while helping in steepening the decline time, would not give a rising forward shock optical emission as we observe.

Yet another option is to interpret the flare as the simultaneous optical emission from an unobserved (because Swift/XRT did not point to the GRB at that time) X-ray flare. X-ray flares are commonly seen in GRB afterglows, at times typically 1000-10000 sec (rest frame) after the GRB (Chincarini et al. 2007). In our case, the early occurrence would be on the short side of this distribution, still consistent with this distribution. The presently generally accepted explanation for the X-ray flares is that they are due to late-time internal shocks (Kocevski et al. 2007), in particular either with a low Γ -difference (so they collide late), or ejected with a large time difference (late-time activity of the engine). For both cases, one expects that the rise time is (much) shorter than the decay time: The rise time is basically the time it takes for the reverse shock of that collision to travel through the thickness of the shell. The decay time is due to the curvature effect, becoming important whenever the radius of the shell exceeds the shell thickness. Thus, if we require that the decay time is not larger than the rise time (as we observe), then the shell radius must be of the order of the shell thickness - and this is valid only very early after the GRB, thus incompatible with our late-time occurrence. Also, simultaneous Swift/UVOT observations of the many X-ray flares have not revealed such flaring activity in the UV/optical domain. Thus, we consider it unlikely that the optical flare in GRB 080129 is the optical counterpart of an unseen X-ray flare.

Invoking a late internal shock between shells which have not produced gamma-ray emission, and collide at large radii, is another option. While this scenario has been already proposed to explain the early optical emission of GRBs 990123, 041219 and 060111B (Wei 2007), it requires that the late ejections have, for some reason, very high Γ of order 800–1000, without producing gamma-ray emission. This Γ value is well above the measured $\Gamma \lesssim 120$ of the

main burst.

Finally, our light curve has, at first glance, some resemblance to that of GRB 041219A, a long-duration ($T_{90} = 520$ sec) burst for which PAIRITEL obtained infrared photometry starting before the end of the burst (Blake et al. 2005). In that case, the first flare, occurring before the end of the burst emission, was associated to the internal shock that produced the GRB; however, the note added in proof implies that a re-analysis of the data showed less evidence for the rising part. Thus, it remains open whether this emission was indeed a flare, or some slower-decaying prompt emission. The second flare at $3 \times T_{90}$ was associated with the reverse shock. The rise and decline times of this second flare, $\beta_{rise} = 6.1 \pm 2.9$ and $\beta_{decline} = -3.4 \pm 2.8$ are fully consistent even with the simplest model of a reverse shock, while our values for GRB080129 are not. Thus, the similarity between the observed optical/infrared light curves of GRB 041219 and 080129 ends with the global structure of multiple peaks in the light curves, but does not provide clues to solve the discrepancies in the case of GRB 080129.

3.4.2. *The likely cause of the flare*

The best match of the observed properties of the flare in GRB 080129 with theoretical predictions is with residual collisions in GRB outflows (Li & Waxman 2008). Internal collisions at small radii, which produce the γ -ray emission, have been proposed to lead to residual collisions at much larger radii where the optical depth to long-wavelength photons is much lower. If the bulk Lorentz factor is large, the optical emission is delayed by only fractions of a second with respect to the γ -rays, and thus can explain the prompt optical emission which has been seen so far in a few GRBs like GRB 041219A, 050820A or 080319B. In the case of GRB 080129, $\Gamma \lesssim 120$, and the delay time can be longer than the duration of the burst (in such case the electrons that radiate in the optically emitting region do not cool because of up-scattering the GRB photons). Li & Waxman (2008) showed that the radius at which the (observer-frame) NIR $\sim 10^{14}$ Hz radiation becomes optically thin is $R_{\text{NIR}} \sim 7.3 \times 10^{15} L_{k,52}^{1/2} \Gamma_2^{1/2}$ cm, resulting in a delay $\tau \sim R_{\text{NIR}}/2\Gamma^2 \sim 12 L_{k,52}^{1/2} / \Gamma_2^{3/2}$ sec. Assuming that the kinetic luminosity of the flow $L_k \sim 10 L_\gamma \sim 10^{53}$ erg/sec (in fact the very long phase of optical emission between 1-3 days after the GRB with a luminosity similar to that of the burst itself implies a large kinetic energy), the delay time can be $\tau \sim 100$ sec if $\Gamma \sim 50$. The predicted spectral slope above the self-absorption frequency is $\nu F_\nu \sim \nu^{0.5}$, and $\nu^{7/6}$ below, consistent with our measured values of 0.57 and 1.2, respectively (rising part of the flare). Also, the predicted ratio of $F_\gamma/F_{opt} \sim 500$ compares well with the observed ratio of 1000.

Given this tantalizing coincidences, we analyzed in more detail the shape of the optical

flare light curve. It turns out that it can be well described by the superposition of two Gaussian profiles (Fig. 1; note that log Gaussians or fast-rise-exponential-decay curves do not fit). We speculate that these are the direct signatures of the residual collisions. Looking at the γ -ray light curve from Swift/BAT (Fig. 5), one can recognize two pulses, the first with FWHM = 11 sec, the second with FWHM = 6 sec. It is interesting to note that the ratio of the FWHM of these pulses is two, identical to the corresponding ratio of the optical pulses. Given that just the sequence of broad/narrow pulse has inverted, one could speculate even further that the shell causing the narrow, second peak in γ -rays had a slightly higher Γ and took over the shell causing the broader, first γ -ray pulse, thus leading to the optical flare.

A caveat with this interpretation comes from the observed fast variability of the flare. Residual collisions are expected to result in a smooth optical lightcurve that varies on the delay timescale. Alternatively the flare may be powered by dissipation of Poynting flux in a localized “hot spot” in strongly magnetized ejecta (Lyutikov 2006; Giannios 2006). In this picture the fast variability is the result of the small emitting volume. The observed fluence of the flare is comparable to the energy available in the volume of the hot spot as constrained by the observed fractional duration of the flare $\delta t_f/t_f \sim 0.15$ (Giannios 2006). The energy contained in the “hot spot” is $E_{\text{HS}} \sim E_{\gamma,iso}(\delta t_f/t_f)^3 \sim 3 \times 10^{50}$ erg (assuming again that the total energy in the ejecta is ~ 10 times larger than the $E_{\gamma,iso}$) In this scenario of a “hot spot”, the radiation would also be strongly polarized - a prediction which can help to distinguish the above two models by future observations of similar phenomena.

4. Conclusions

If more detailed theoretical investigation of the properties of residual collisions and the comparison of their predictions with our data will support our interpretation of the observed flare to be correct, then the delay time between gamma-ray and optical flare provides an independent way of determining the Lorentz factor Γ . Moreover, further parameters of the blast wave can be determined, which were not constrained by observations so far, such as the distance of the residual collisions, the ratio of radiation to magnetic field energy (via the ratio of inverse Compton and synchrotron emission), and the ratio of kinetic to gamma-ray energy. This offers the hope to finally measure the energetics of gamma-ray bursts beyond the rare cases of calorimetry with radio observations.

We are grateful to Pierre Cox, the IRAM Director, for granting DDT time at the 30m telescope, as well as to C. Thum and S. Leon (also IRAM) for getting the observations performed. This work is partly based on observations collected at the European Southern

Observatory, Chile under proposal ESO No. 280.D-5059.

REFERENCES

- Akerlof C., Balsano R., Barthelmy S., et al. 1999, *Nature* 398, 400
- Björnsson G., Gudmundsson E.H., Johannesson G., 2004, *ApJ* 615, L77
- Blake C.H., Bloom J.S., Starr D.L., et al. 2005, *Nat.* 435, 181
- Bloom J.S., Frail D.A., Kulkarni S.R., 2003, *ApJ* 594, 674
- Bloom J.S., 2008, *GCN Circ. #7229*
- Chincarini G., Moretti A., Romano P., et al. 2007, *ApJ* 671, 1903
- Dickey, J. M., Lockman, F. J. 1990, *ARAA* 28, 215
- Giannios D. 2006, *A&A* 455, L5
- Greiner J., Bornemann W., Clemens C., et al. 2008, *PASP* 120 405
- Holland S.T., 2008, *GCN Circ. #7227*
- Immler S., Burrows D.N., Chester M.M., et al. 2008, *GCN Circ. 7226*
- Kaneko Y., Preece R.D., Briggs M.S., Paciesas W.S., Meegan C.A., Band D.L., 2006, *ApJ Suppl.* 166, 298
- Klotz A., Gendre B., Stratta G., et al. 2006, *A&A* 451, L39
- Kobayashi S., 2000, *ApJ* 545, 807
- Kocevski D., Butler N.R., Bloom J.S., 2007, *ApJ* 667, 1024
- Kreysa, E., et al. 1998, *Proc. SPIE*, 3357, 319
- Krühler T., Loew S., Greiner J., et al. 2008, *GCN Circ. #7231*
- Lazzati D., Rossi E., Covino S., Ghisellini G., Malesani D. 2002, *A&A* 396, L5
- Lazzati D., 2005, *MN* 357, 722
- Li Z., Waxman E., 2008, *ApJ* 674, L65

- Liang E.-W., Zhang B.-B., Zhang B., 2007, ApJ 669, 565
- Lyutikov M., 2006, New Journal of Phys. 8, Issue 7, 119
- Meszaros P., Rees M. 1997, ApJ 476, 232
- Meszaros P., Rees M., 1999, MN 306, L39
- Molinari E., et al. 2007, A&A, 469, L13
- Panaitescu A., Kumar P., 2000, ApJ 543, 66
- Panaitescu, A., 2007, MNRAS 380, 374
- Racusin J.L., Karpov S.V., Sokolowski M., et al. 2008. Nat. 455, 183
- Rykoff E., et al. 2004, ApJ 601, 1013
- Sari R., Piran T., 1999a, ApJ 517, L109
- Sari R., Piran T., 1999b, ApJ 520, 641
- Sari R., Piran T., Halpern J.P., 1999, ApJ 519, L17
- Vestrand W., et al. 2005, Nat. 435, 178
- Vestrand W., et al. 2006, Nat. 442, 172
- Wei D.M. 2007, MN 374, 525

Table 1: Sub-mm measurements of GRB 080129 with MAMBO.

Date	LST (hr)	MJD	Flux (mJy)	Exp.time (sec)	Opacity	Elev (deg)	Scan
2008-01-30	6.1	54495.90	2.98 ± 0.63	2358	0.20–0.21	43-45	1-2
2008-01-31	7.9	54496.98	1.27 ± 0.47	5097	0.23–0.29	43-29	3-7
2008-02-03	9.3	54499.02	0.50 ± 1.16	1415	0.27	35-33	8-9
2008-02-06	8.6	54502.99	-0.40 ± 0.55	3540	0.20–0.24	30-40	10-12
2008-02-10	10.4	54506.05	0.55 ± 1.14	1170	0.29–0.33	22-25	13

Table 2: Fit parameters of the combined Swift-XRT/GROND/MAMBO SEDs. The normalisation is in $\text{ph}/\text{cm}^2/\text{s}/\text{keV}$, and only a break between GROND and XRT data is fit, with the break energy fixed at 0.1 keV. Leaving the break energy free results in best-fit values between 0.05-0.25 keV with large errors. We have no evidence that the break energy moved in time, neither between the GROND and XRT bands, nor through the GROND band towards shorter frequencies.

Interval	Time (ksec post-GRB) GROND/XRT/MAMBO	Low-energy power law photon index	High-energy power law photon index	Norm	$\chi^2_{\text{red}}/\text{d.o.f}$
1	2.96-4.46/3.22-4.48/-	1.41 ± 0.13	2.12 ± 0.33	6.45E-03	0.94/10
2	4.48-6.04/4.48-5.80/-	1.39 ± 0.11	2.33 ± 0.38	5.93E-03	0.97/7
3	68-170/68-149/141-143	1.57 ± 0.06	$2.36^{+1.01}_{-0.58}$	1.41E-03	0.81/3
4	248-328/250-350/232-237	1.60 ± 0.09	$1.92^{+1.50}_{-0.10}$	4.93E-04	0.41/4

Table 3: Fit parameters of the combined Swift-XRT/GROND/MAMBO SEDs when enforcing two breaks, one between MAMBO and GROND, and the other one between GROND and Swift/XRT. The normalisation is in $\text{ph}/\text{cm}^2/\text{s}/\text{keV}$. The break energies have been fixed at $5\text{E-}5$ keV (1.2 mm) and 0.5 keV, respectively.

SED	Gamma1	Gamma2	Gamma3	Norm	$\chi^2_{\text{red}}/\text{d.o.f}$
SED III	1.47 ± 0.14	1.69 ± 0.13	2.31 ± 0.23	$5.97\text{e-}3$	0.38/4
SED IV	1.53 ± 0.24	1.67 ± 0.21	2.10 ± 0.38	$1.08\text{e-}3$	0.43/4

Table 4: Fit parameters of the GROND SED data alone during the 4 intervals as shown in Fig. 2. For the flare SEDs a break is required, and has been fixed at 1500 nm. β_1 and β_2 are the low- and high-energy power law photon indices, respectively.

Time	β_1	Break nm	β_2	Norm μJy
1. flare peak	0.57 ± 0.27	1500	1.20 ± 0.10	363 ± 17
2. flare decay	0.99 ± 0.26	1500	1.87 ± 0.09	164 ± 7
3. rising AG	1.27 ± 0.04	–	–	10.9 ± 2.4
4. peak AG	1.52 ± 0.04	–	–	4.2 ± 0.9

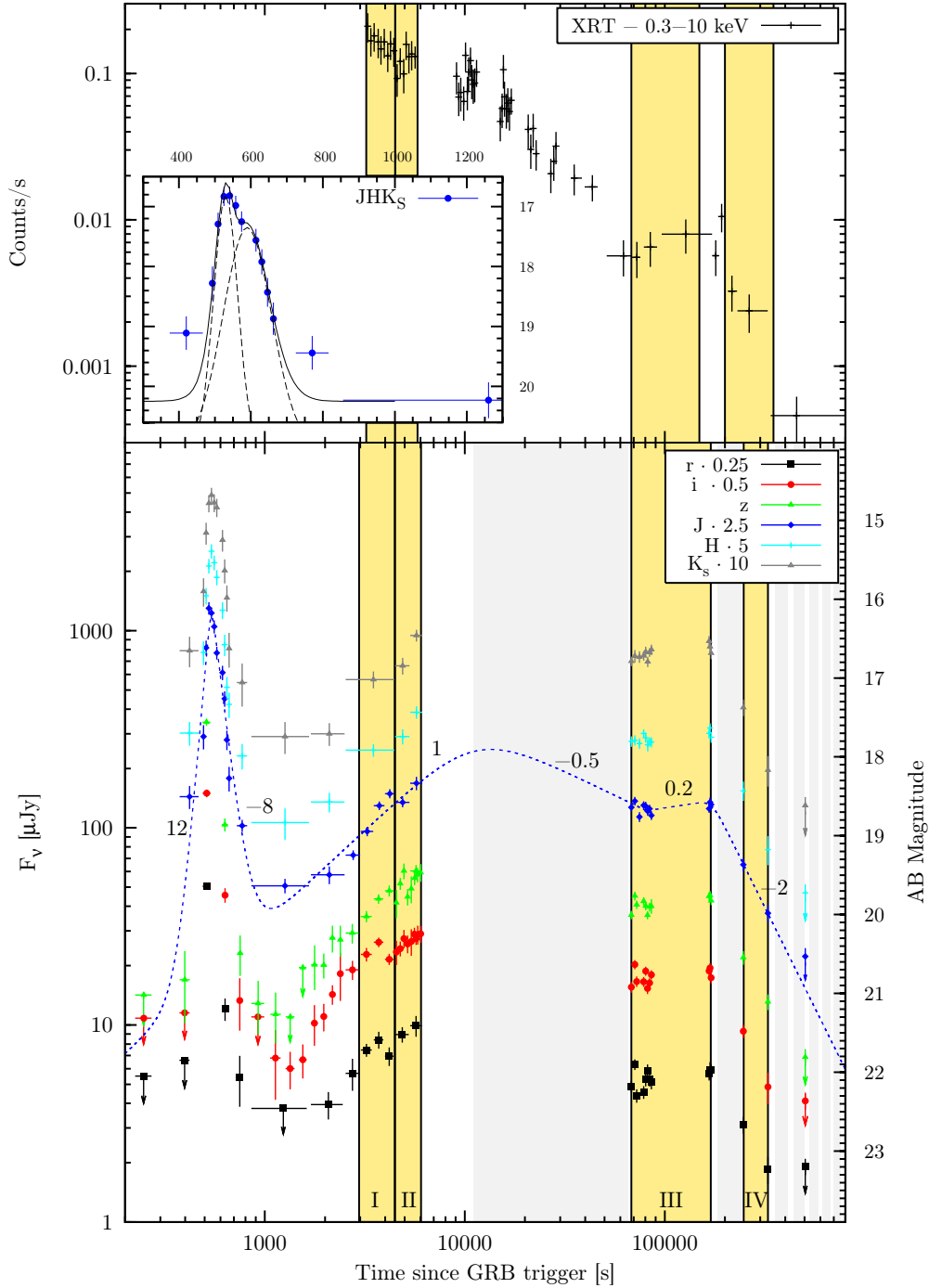


Fig. 1.— Optical light curve of the afterglow of GRB 080129 obtained with the 7-channel imager GROND at the 2.2m telescope on La Silla / Chile (bottom) and the X-ray light curve as measured with the XRT onboard Swift (top). NIR exposures have been co-added until at least $S/N=5\sigma$ was reached. During the optical/NIR flare at ~ 500 sec, the individual 10 sec integrations are shown. The inset in the top panel shows the flare in the three NIR channels co-added, and modelled by the sum (full line) of two (dashed lines) Gaussians with FWHM of 77 and 157 sec, respectively. The J -band data have been fit by the sum of several power law segments shown as dashed line. Numbers at this line indicate the temporal power law indices α . The yellow-shaded areas are the time intervals of the SEDs as detailed in Tabs. 2, 3 and 4.

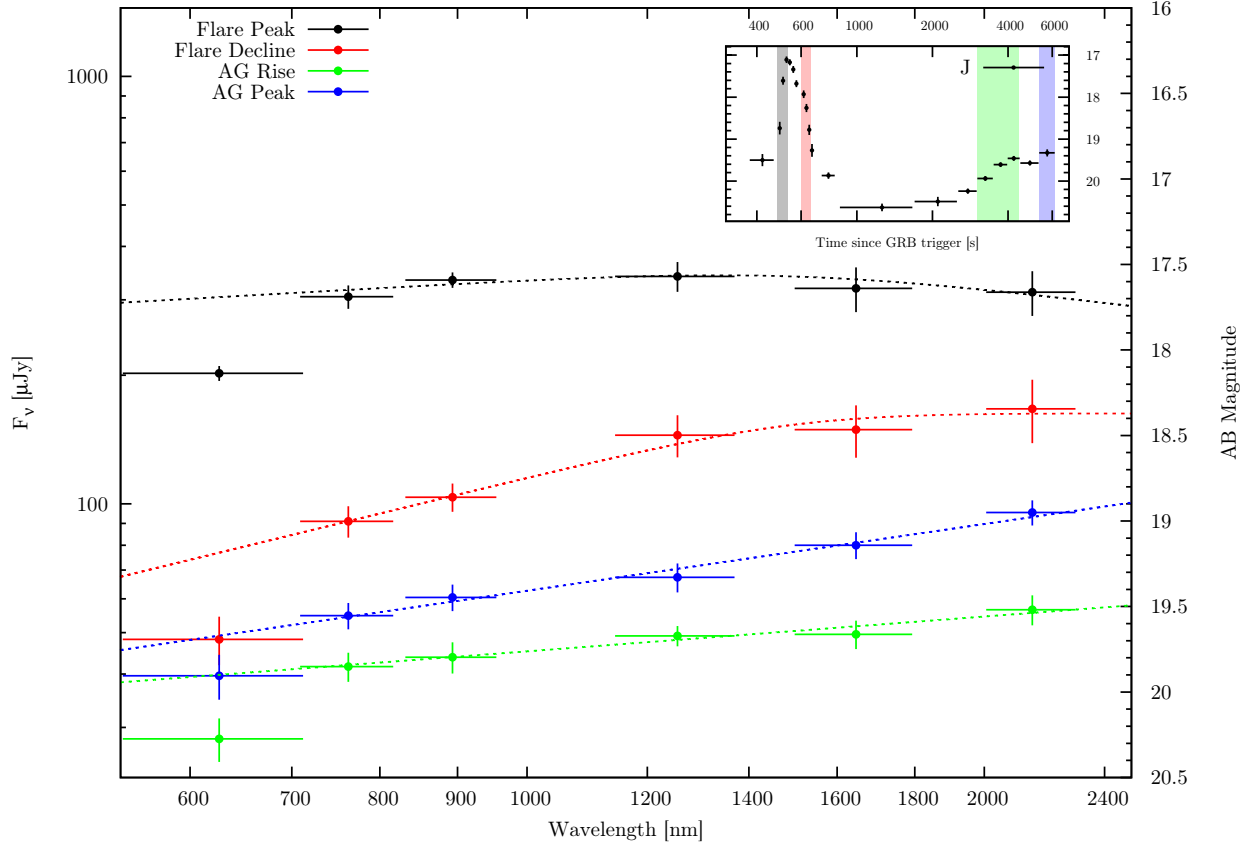


Fig. 2.— Spectral energy distribution (SED) at four different times (see inset; from top to bottom): (i) the peak of the flare (ii) the decay part of the flare (iii) the maximum of the afterglow emission, and (iv) the rising part of the afterglow emission as measured by GROND. The Ly- α line affects the r' -band, and has not been included in the fit. The burst location is at galactic latitude -1.42 deg, thus the foreground galactic hydrogen column is $N_{\text{H}} = (6.7\text{-}7.5) \cdot 10^{21} \text{ cm}^{-2}$ (Dickey & Lockman 1990), corresponding to a Galactic visual extinction of $A_V = 3.5\text{-}4.1$ mag. Our best-fit extinction is $A_V = 3.4$ mag, and all measured magnitudes have been corrected for this extinction. The power law photon indices are given in Tab. 4. The break in the flare spectrum violates one of the assumptions made for deriving the $\alpha = 2 + \beta$ relation for the curvature effect; thus, the curvature effect can not be tested for the observed optical flare.

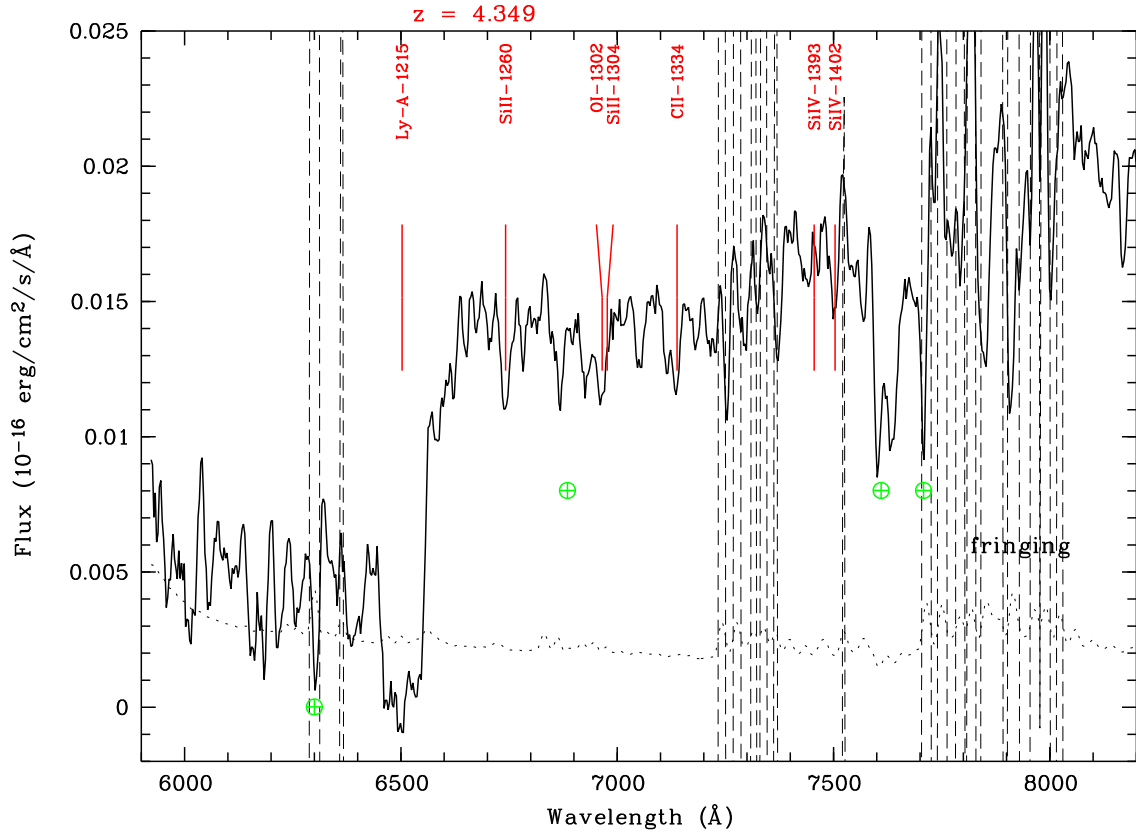


Fig. 3.— Optical spectrum of the afterglow of GRB 080129 obtained with FORS1/VLT on Jan 30, 2008. The Ly α line is clearly visible at 6500 Å, and places GRB 080129 at a redshift $z=4.349$ (or larger). Some expected metal lines (in the rest frame) are indicated. The dotted line is the noise spectrum, and the vertical dashed lines mark regions of strong sky lines.

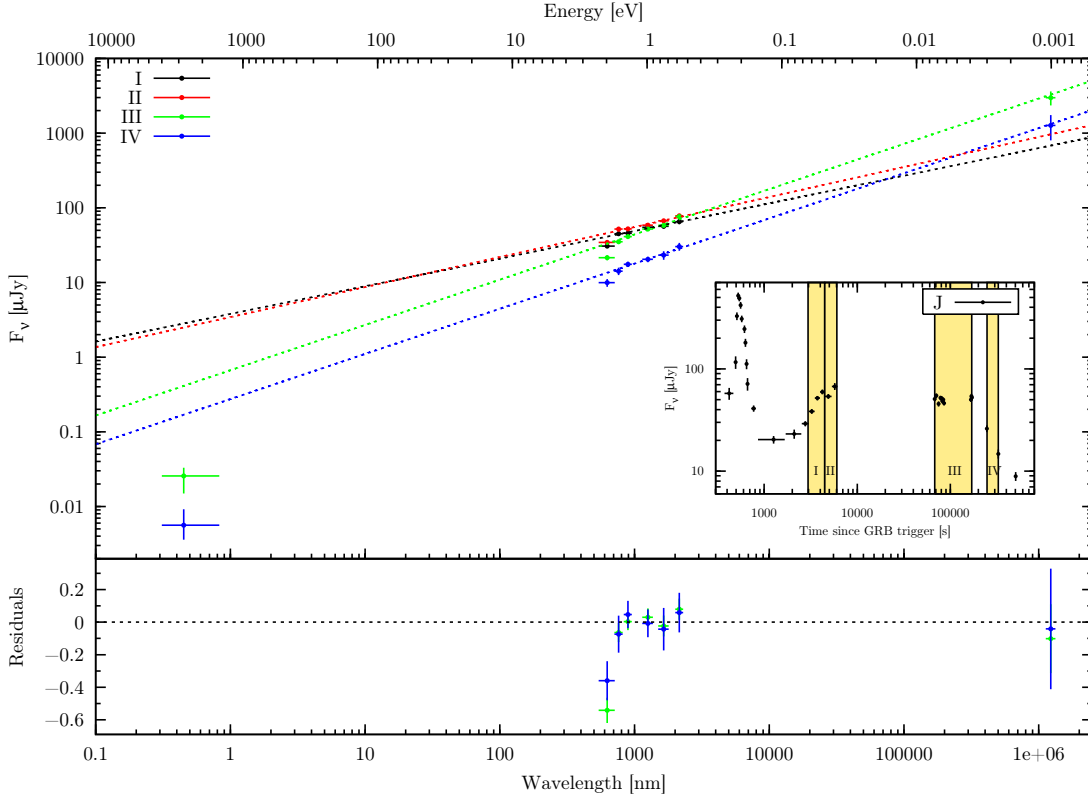


Fig. 4.— Broad-band spectrum of GRB 080129 at different epochs (see inset and legend), combining GROND data (center) with Swift/XRT (left) and MAMBO (top right). The best-fit photon indices are 2.66 ± 0.12 at wavelengths shorter than 400 nm, and 1.62 ± 0.03 above. The best-fit extinction of the optical/NIR fluxes is $A_V = 3.4 \pm 0.1$ mag, and the neutral hydrogen absorption $N_H = 6 \times 10^{21} \text{ cm}^{-2}$ which are nicely consistent with the canonical galactic conversion. The X-ray data are a factor ~ 10 below the power law connecting GROND and MAMBO, and thus a break in the spectrum is required.

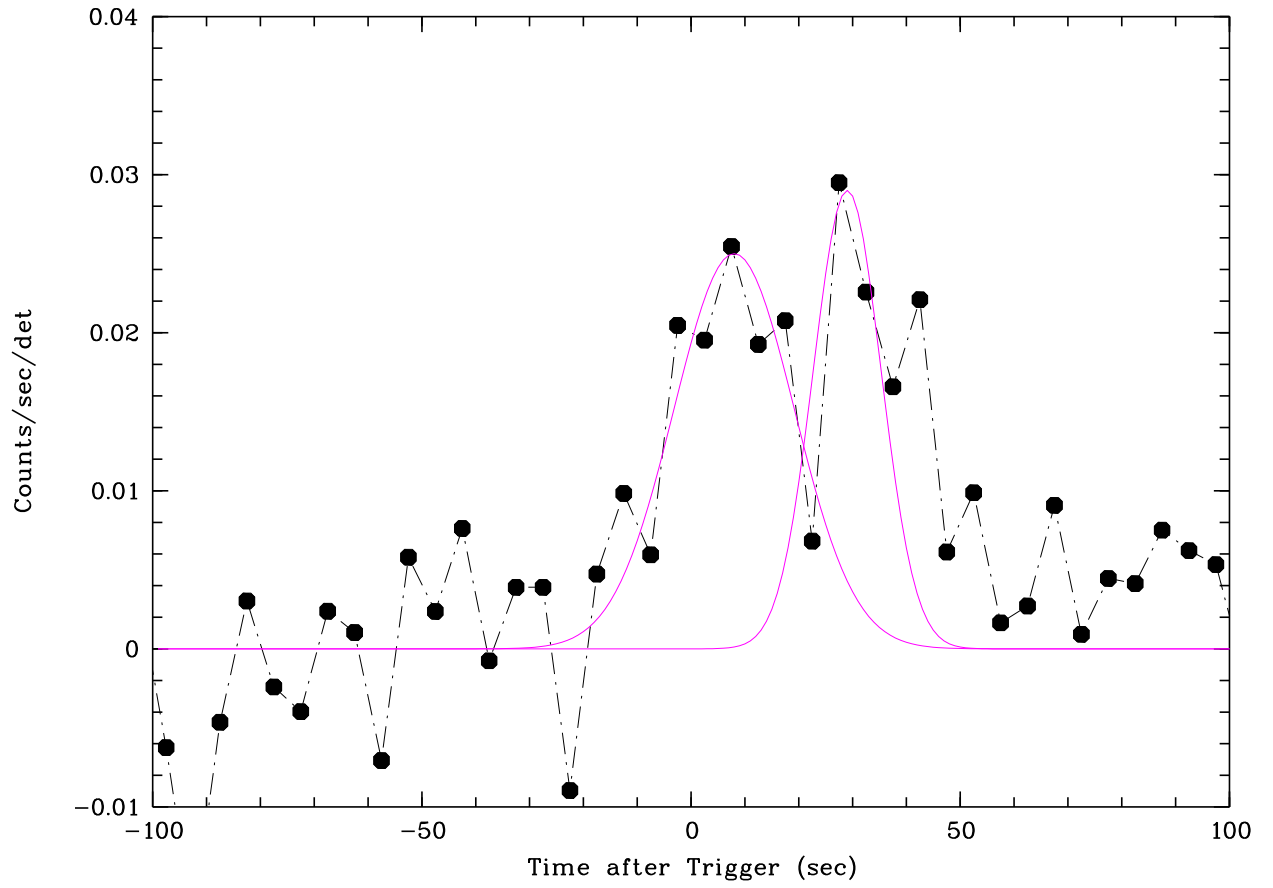


Fig. 5.— Swift/BAT light curve of GRB 080129, rebinned with $S/N=5$. Overplotted are the two peaks, modelled with two Gaussians of 11 sec and 6 sec FWHM, respectively.